

**ADVANCED
HEALTHCARE
MATERIALS**

Supporting Information

for *Adv. Healthcare Mater.*, DOI: 10.1002/adhm.201400035

Soft Robotic Concepts in Catheter Design: an On-Demand
Fouling-Release Urinary Catheter

*Vrad Levering, Qiming Wang, Phanindhar Shivapooja,
Xuanhe Zhao,* and Gabriel P. López**

Copyright WILEY-VCH Verlag GmbH & Co. KGaA, 69469 Weinheim, Germany, 2013.

Supporting Information

Soft Robotic Concepts in Catheter Design: an On-demand Fouling-release Urinary Catheter

Vrad Levering, Qiming Wang, Phanindhar Shivapooja, Prof. Xuanhe Zhao*, and Prof. Gabriel P. López*



Figure S1. Growth and characterization of mature *P. mirabilis* crystalline biofilms on flat silicone substrates. (a) Schematic of the flow system. The silicone samples were submerged in (b) the modified drip flow reactor^[1] and inoculated with a 4 hour culture of *P. mirabilis*. After allowing the bacteria to adhere for 1 hour, artificial urine with 1% tryptic soy broth was pumped at 0.5 mL min^{-1} through the drip flow reactor and over the flat silicone samples. The reactor was maintained at 37°C by mini-incubator. A mature crystalline biofilm grew over approximately 42 hours. (c) SEM of the resultant planar biofilm shows large crystals and microcrystal aggregates typical of mature *P. mirabilis* biofilms observed in catheters removed from infected patients.^[2]

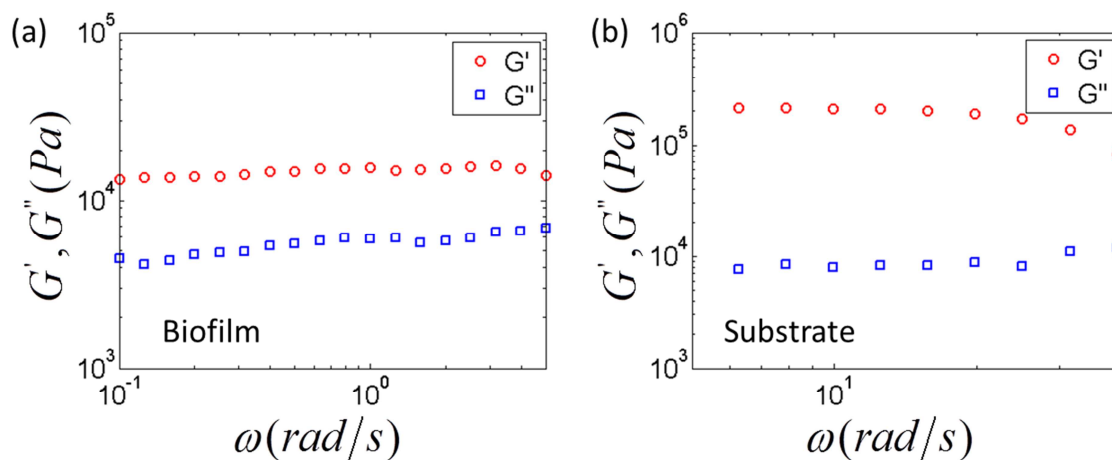


Figure S2. Storage modulus G' and loss modulus G'' of mature *P. mirabilis* crystalline biofilms and the silicone substrate as a function of frequency. (a) *P. mirabilis* crystalline biofilms appeared to demonstrate predominantly elastic properties; the storage modulus was higher than the loss modulus and was relatively constant over the frequency range tested.^[3] (b) Storage and loss moduli of silicone substrate.

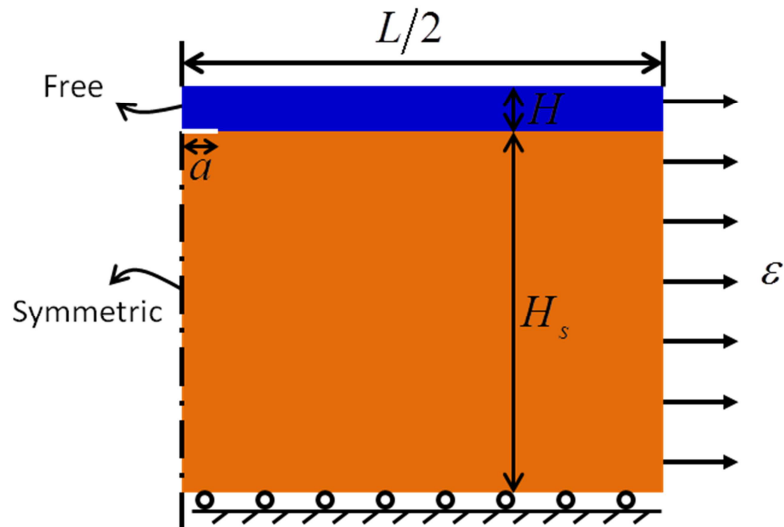


Figure S3. Schematic illustration of the boundary conditions for the finite element model for calculating energy release rate in Figure 3c. H is the thickness of the biofilm, H_f is the thickness of the substrate, L is the crack width illustrated in Figure 3b, a is the crack length on the biofilm-substrate interface, and ε is the applied strain. Boundary and load conditions include: symmetric boundary condition on the left surface of the substrate, a sliding condition on the bottom of the substrate, a horizontal displacement of $\varepsilon L/2$ applied on the right surfaces of the biofilm and the substrate, and free boundaries on other surfaces.

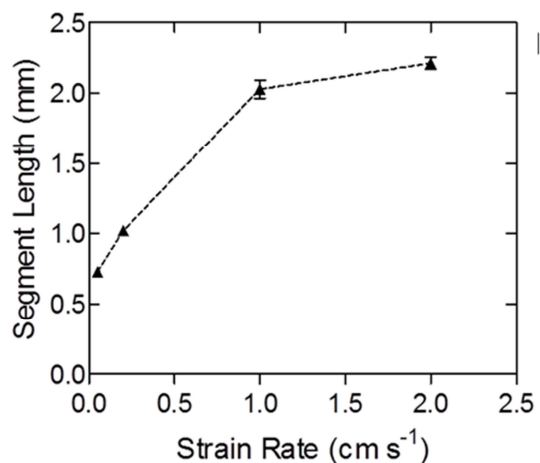


Figure S4. Segment length increases with increasing strain rate. Segment length from representative images at 100% strain (such as those in **Figure 3 B** and **C**). Five lines were drawn lengthwise (equally spaced along the width of the sample) on each image, and segment length was measured along the lines using ImageJ. Error bars provide the standard error of the mean of greater than 30 measurements per image.

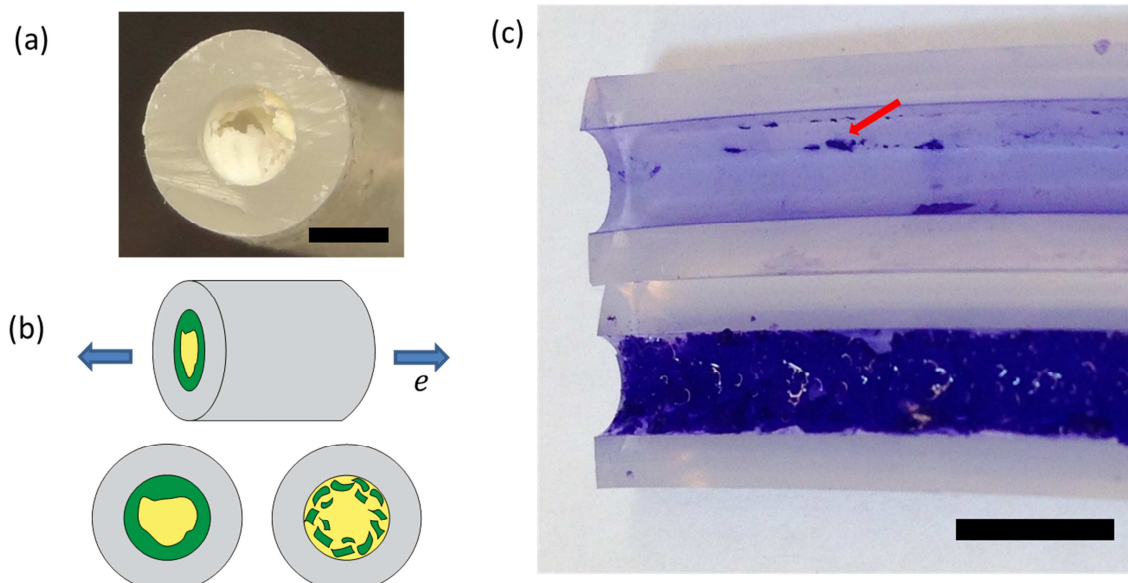


Figure S5. Debonding of mature *P. mirabilis* crystalline biofilms via applied strain to silicone tubing substrates. (a) Representative image of crystalline biofilm occluding a portion of silicone tubing. Using similar growth methods to the flat configuration, mature crystalline biofilm was grown in silicone tubing (6.35mm inner diameter silicone tubing, VWR). Bar indicates 2.5 mm. (b) Diagram of how tensile strain applied to substrate debonds a biofilm within a tube. Unidirectional strain was applied axially. The cross section on the left represents a tube with biofilm grown on the main lumen; the cross section on the right represents the same tube after axial strain was applied to the substrate. Biofilm becomes debonded from the luminal surface and available for easy removal via rinse. (c) Image of sliced tubing sample subjected to 50% strain 10 times (top) and unstrained control (bottom) after rinsing. Arrow indicates example of remaining islands of biofilm of partial-thickness. Strained samples were stretched at 1.7 cm s^{-1} using a LRX tensile tester. Samples were then rinsed at 4 mL min^{-1} before crystal violet staining. SEM comparison of flat and tubular silicone surfaces used for these experiments confirmed similar surface topographies. Scale bar indicates 5 mm.

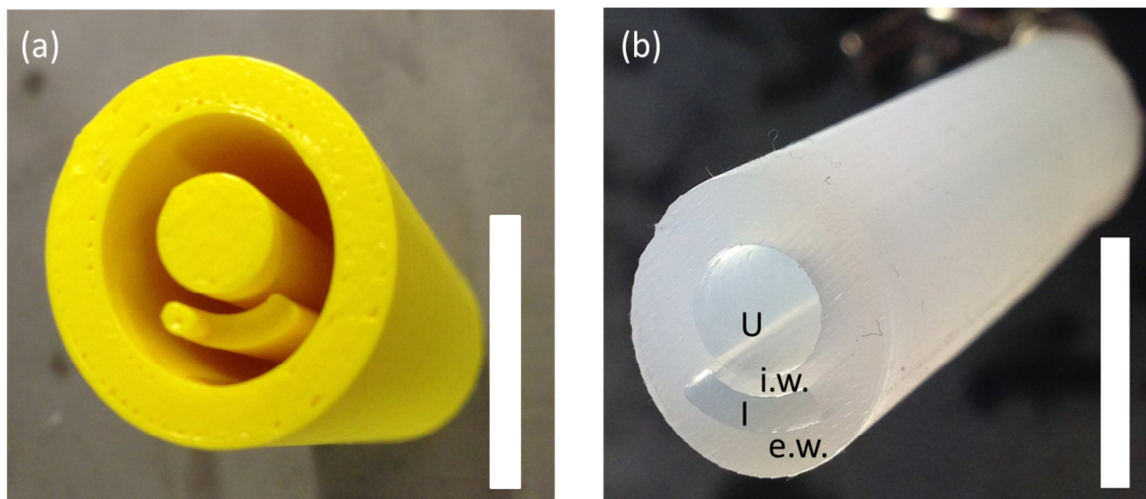


Figure S6. Construction of an active fouling release, proof-of-concept prototype of a section of silicone urinary catheter. (a) 3D printed mold patterns were generated using Solidworks 2011 and then printed on a Dimension sst 1200es 3D printer. Silicone (Dragon Skin 0020 or Ecoflex 0050) was poured into the mold and (b) resultant silicone prototypes were removed from the mold upon curing. “U” denotes the main urine drainage lumen, “I” denotes the inflation lumen, “i.w.” denotes the inflation wall, and “e.w.” denotes the external wall. The inflation lumen was sealed at the ends of the prototypes before experimentation. When using Dragon Skin 0020 silicone, the ratio of external wall to inflation wall thicknesses shown (approximately 3:1) was sufficient to direct inflation inwards. When using Ecoflex 0050 silicone, prototypes required an additional inelastic sheath to prevent bulging of the external wall. Ecoflex 0050 was chosen for *in vitro* biofilm testing due to its superior pour performance and consistently successful molding. Scale bar represents 1 cm.

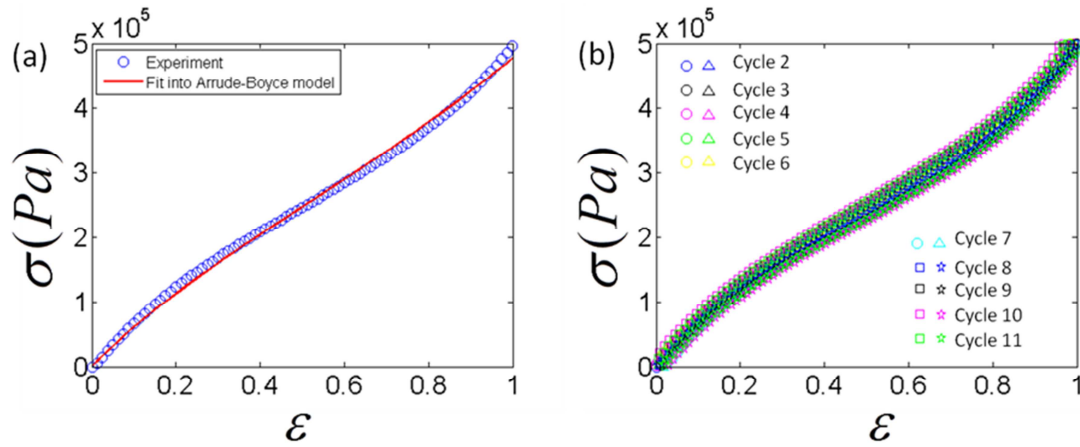


Figure S7. (a) Nominal stress *vs.* strain curve of Dragon skin 0020 was fit to the Arrude-Boyce model, $\sigma = \mu_s(\lambda - \lambda^{-2})(1 + \frac{I}{5n} + \frac{11I^2}{175n^2} + \dots)$, where σ and $\lambda = 1 + \varepsilon$ are the nominal stress and stretch for uniaxial tension, $I = \lambda^2 + 2\lambda^{-1}$, and n is a parameter that accounts for the stiffening effect.^[4] The fitted shear modulus is $\mu_s = 221$ kPa, and the exponent was fitted as $n = 0.27$. (b) Cycling test of Dragon skin 0020 shows negligible hysteresis after the first strain loading cycle. Silicone samples (flat and proof-of-concept prototypes) were prestrained or preactuated at least once prior to experimentation.

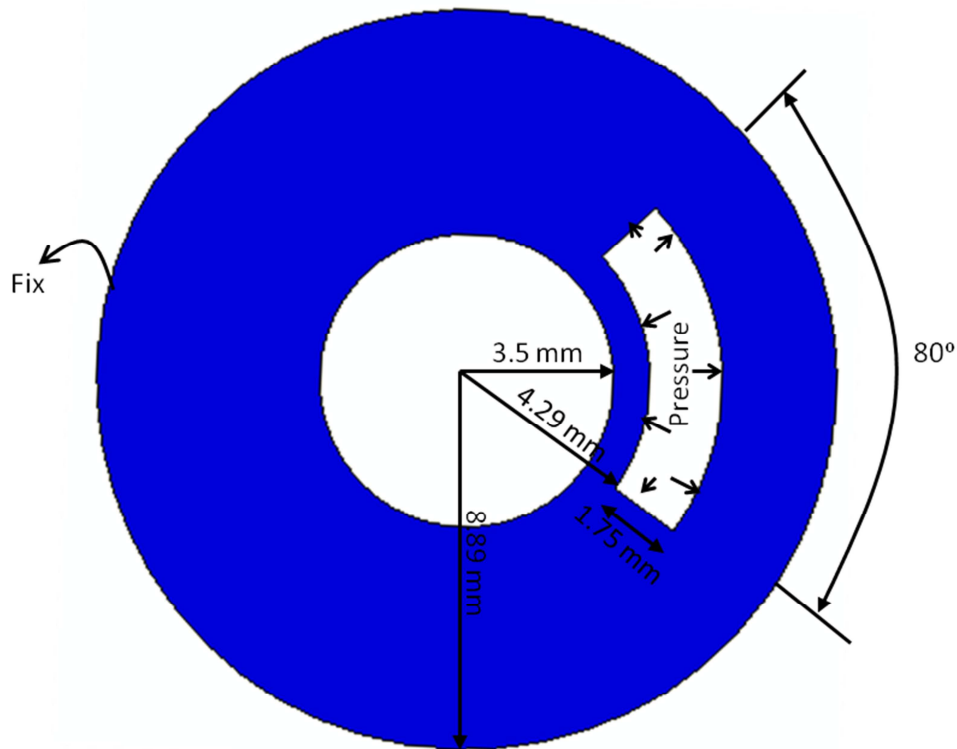


Figure S8. Schematic illustration of the boundary conditions for the finite element model for calculating strain at the luminal surface of proof-of-concept prototypes (Dragon Skin 0020) in Figures 4c and 4d. The outer surface the model was fixed, and pressure was applied on the inner surface of the inflation lumen.

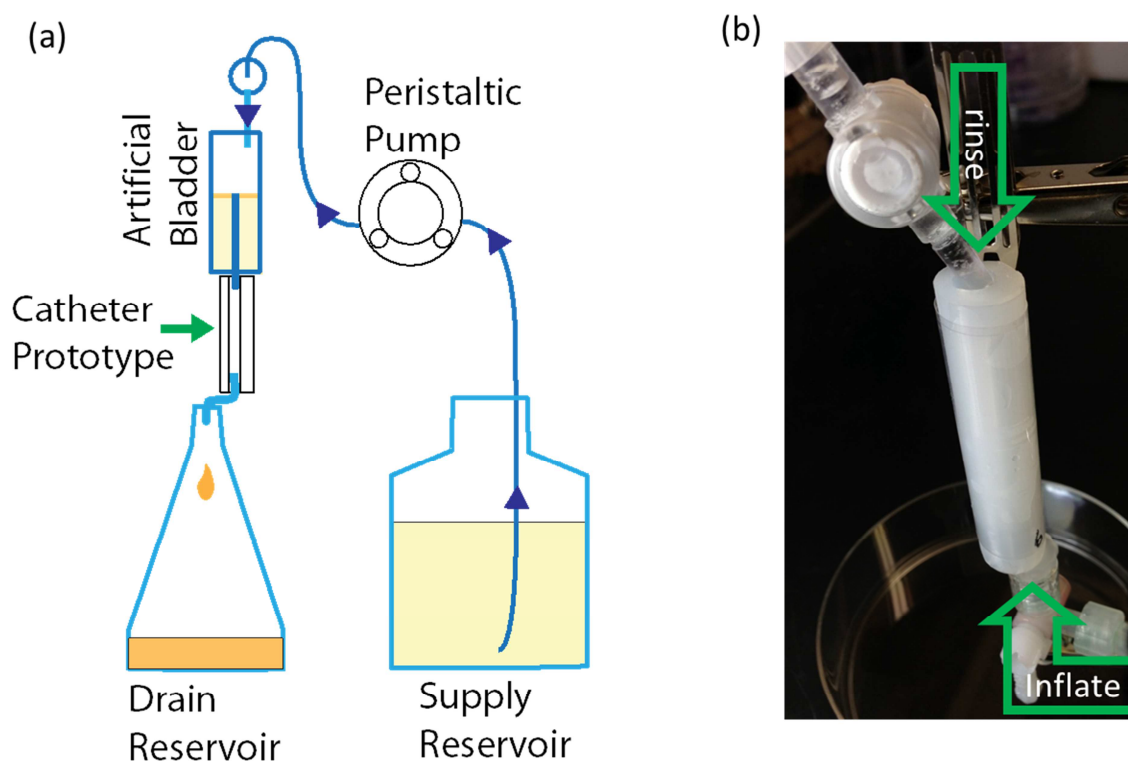


Figure S9. Biofilm growth and testing setup for urinary catheter proof-of-concept prototypes. (a) Schematic of biofilm growth system that uses an “artificial bladder”^[5] to supply infected urine to the proof-of-concept prototypes. The artificial bladder is a vessel modified with a glass tube penetrating the bottom and extending approximately 4 cm into the vessel, which thereby maintains a residual volume of 30 mL in the artificial bladder. The artificial bladder and prototypes were inoculated with a 4 hour culture of *P. mirabilis*. After allowing the bacteria to adhere for 1 hour, artificial urine with 1% tryptic soy broth was pumped at 0.5 mL min^{-1} into the artificial bladder and through the prototypes. As artificial urine media was fed into the artificial bladder the media overflowed into the glass tube, where it then fed down the main drainage lumen of the catheter prototypes. The bladder and prototypes were maintained at 37°C by mini-incubator. A mature crystalline biofilm grew over approximately 42 hours. (b) Rinsing test setup for prototypes after biofilm growth. After carefully removing the prototypes from the biofilm growth system, a DI water rinse supplied at 4 mL min^{-1} flowed downward through the prototype main urine drainage lumen for 1 minute. Prototypes designated for actuation were hydraulically inflated 10 times at a rate of 0.1 s^{-1} approximately 30 seconds into the rinse. Hydraulic inflation was applied to the inflation lumen through an inflation port fixture on the bottom end of the prototype. The rinse effluent was collected for analysis and the prototype was then removed for inspection.

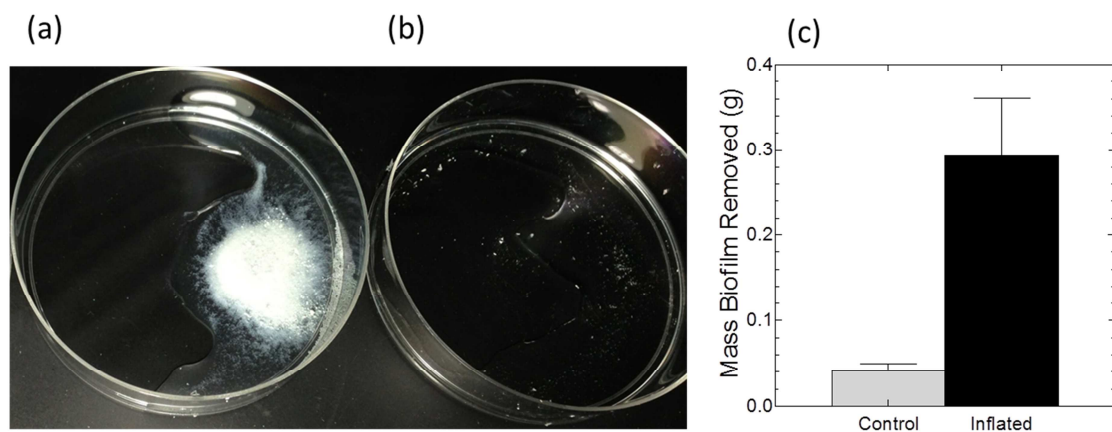


Figure S10. Dramatic release of biofilm into the effluent from inflated proof-of-concept prototype urinary catheters. (a) Representative optical image of effluent from 3 prototypes each actuated $10\times$ during rinsing (4 mL min^{-1} through the prototype main urine drainage lumen for 1 minute); effluent contained visible biofilm debris. (b) Representative effluent from 2 un-actuated control prototypes had minimal biofilm debris, implying that control prototypes retained biofilm after rinsing alone. (c) The effluent was collected, centrifuged, and the excess liquid was aspirated. Figure shows hydrated mass of biofilm collected. Data represents mean \pm standard error of the mean.

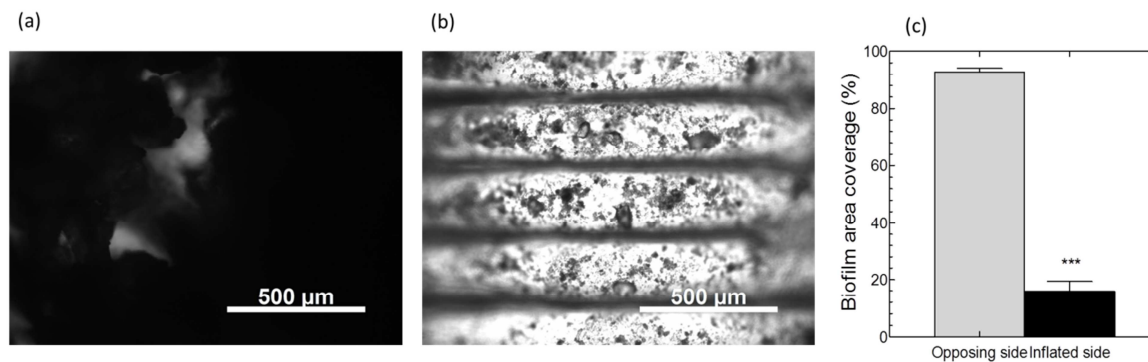


Figure S11. Microscopic observation of debonding of biofilm from the main urine drainage lumen of catheter section prototypes. (a) Microscope image of surface of control prototype main lumen covered with biofilm after rinsing and (b) Microscope image of inflated prototype main lumen with biofilm removed after inflation and rinsing. Note: Horizontal bars visible across the inflation wall are “ribs” around the lumen that are due to the 3D printing process used to form the mold. (c) ImageJ was used to analyze the images, and statistical comparison to the opposing side of the catheter lumen showed that inflation debonded the biofilm from the area of the luminal wall subjected to inflation. Comparison was statistically significant both with ($p < 0.006$) and without ($p < 0.0009$) rib artifacts removed from images. Data represents mean \pm standard error of the mean, $N=4$.

Table S1. Hydraulic inflation profile for proof-of-concept prototypes of urinary catheter sections.

Inflation Volume (mL water)	Strain (%)
0	0.0
1	13.0
1.3	34.7
1.6	38.8
1.7	39.1

References

- [1] D. M. Goeres, L. R. Loetterle, M. A. Hamilton, R. Murga, D. W. Kirby, R. M. Donlan, *Microbiology* **2005**, *151*, 757-762.
- [2] D. J. Stickler, S. D. Morgan, *J Hosp Infect* **2008**, *69*, 350-360.
- [3] M. Bol, A. E. Ehret, A. Bolea Albero, J. Hellriegel, R. Krull, *Crit Rev Biotechnol* **2013**, *33*, 145-171.
- [4] J. S. Bergstrom, M. C. Boyce, *Rubber Chemistry and Technology* **1999**, *72*, 633-656.
- [5] D. J. Stickler, N. S. Morris, C. Winters, *Methods Enzymol* **1999**, *310*, 494-501.